CHEMISTRY OF MATERIALS
Article

Chem. Mater. **2009,** *21,* 2875–2885 2875
DOI:10.1021/cm900608d

ZnO with Different Morphologies Synthesized by Solvothermal Methods for Enhanced Photocatalytic Activity

Linping Xu,[†] Yan-Ling Hu,[‡] Candice Pelligra,[†] Chun-Hu Chen,[†] Lei Jin,[†] Hui Huang,[†] Shanthakumar Sithambaram,[†] Mark Aindow,[‡] Raymond Joesten,[†] and Steven L. Suib*[,†,‡]

[†]*Department of Chemistry, U-3060, University of Connecticut, Storrs, Connecticut 06269-3060, and* [‡]*Institute of Materials Science, U-3136, University of Connecticut, Storrs, Connecticut 06269*

Received March 3, 2009. Revised Manuscript Received May 1, 2009

ZnO materials with a range of different morphologies have been synthesized via a simple solvothermal method with different solvents. Zinc acetylacetonate was used as the zinc source in such solvothermal syntheses for the first time. XRD data showed that single-phase ZnO with the wurtzite crystal structure was obtained for all the solvents used. FE-SEM imaging showed that ZnO with cauliflower-like, truncated hexagonal conical, tubular and rodlike, hourglass-like, nanorods, and spherical shapes were produced when THF, decane, water, toluene, ethanol, and acetone were used as the solvent, respectively. The TEM data showed that the crystalline ZnO had different growth habits in the different solvents. The optical properties of the as-prepared ZnO materials were investigated by UV−vis absorption and room temperature photoluminescence. Photodegradation of phenol was used as a model reaction to test the photocatalytic activity of the ZnO samples. ZnO samples with different morphologies and crystal growth habits exhibited different activities to phenol degradation. The ZnO material prepared using THF as the solvent showed a nine-times enhancement of the kinetic rate constants over commercial ZnO (0.1496 min^{-1} vs 0.0182 min^{-1}). The influence of the solvents on the morphology of ZnO samples and the effect of the morphologies on the photocatalytic activity are discussed.

1. Introduction

Control of the morphology and size of particulate materials has received increased attention due to the fact they play very important roles in determining magnetic, electrical, optical, and other properties.[1−4] One-dimensional nanostructures, such as nanowires, nanotubes, nanobelts, and nanorods, have attracted intensive interest because of their novel physical properties as well as their potential applications in constructing nanoscale electronic and optoelectronic devices.[5−7] Efforts have been devoted to self-assembly of nanoparticles into two-dimensional (2D) and three-dimensional (3D) well-ordered structures, and several hierarchical architectures.[8−10] Solid templates or structure-directing agents are commonly used to fabricate materials with hierarchical structures,[10,11] but impurities can be introduced from the templates or agents that can affect the properties adversely. There is, therefore, significant interest in developing facile, template-free, solution-based, morphology-controlled approaches to building novel self-generated architectures.

ZnO is a fundamentally important material that has attracted great interest because of a combination of semiconducting, piezoelectric, and pyroelectric properties.[12] ZnO is an intrinsic n-type semiconductor because of the presence of oxygen vacancies and/or zinc interstitials; it exhibits a wide band gap and has a large exciton binding energy. ZnO adopts the wurtzite crystal structure, which has the space group $P6_3mc$ (No. 186) and can be described as an hcp array of Zn atoms at (1/3, 2/3, 0) and (2/3, 1/3, 1/2) in which oxygen atoms occupy half of the tetrahedrally coordinated sites at (1/3, 2/3, 3/8) and (2/3, 1/3, 7/8). The result is a noncentrosymmetric crystal comprised of alternating layers of $^{IV}Zn^{2+}$ and $^{IV}O^{2-}$, which can also be described as sheets of corner-shared $^{IV}ZnO_4^{6-}$ tetrahedra stacked along the *z*-direction in

*To whom correspondence should be addressed. E-mail: steven.suib@uconn.edu.

(1) Li, W.-N.; Yuan, J.; Shen, X.-F.; Gomez-Mower, S.; Xu, L.-P.; Sithambaram, S.; Aindow, M.; Suib, S. L. *Adv. Funct. Mater.* **2006**, *16*(9), 1247.
(2) Xu, L.; Ding, Y.-S.; Chen, C.-H.; Zhao, L.; Rimkus, C.; Joesten, R.; Suib, S. L. *Chem. Mater.* **2008**, *20*(1), 308.
(3) Zhang, H.; Xie, R.; Sekiguchi, T.; Ma, X.; Yang, D. *Mater. Res. Bull.* **2007**, *42*(7), 1286.
(4) Dong, Z. W.; Zhang, C. F.; Deng, H.; You, G. J.; Qian, S. X. *Mater. Chem. Phys.* **2006**, *99*(1), 160.
(5) Goldberger, J.; Sirbuly Donald, J.; Law, M.; Yang, P. *J. Phys. Chem. B* **2005**, *109*(1), 9.
(6) Hullavarad, S. S.; Hullavarad, N. V.; Karulkar, P. C.; Luykx, A.; Valdivia, P. *Nanoscale Res. Lett.* **2007**, *2*(3), 161.
(7) Wang, X.; Liu, J.; Song, J.; Wang, Z. L. *Nano Lett.* **2007**, *7*(8), 2475.
(8) Gu, Z.; Zhai, T.; Gao, B.; Sheng, X.; Wang, Y.; Fu, H.; Ma, Y.; Yao, J. *J. Phys. Chem. B* **2006**, *110*(47), 23829.
(9) Lu, F.; Cai, W.; Zhang, Y. *Adv. Funct. Mater.* **2008**, *18*(7), 1047.
(10) Zhang, T.; Dong, W.; Keeter-Brewer, M.; Sanjit, K.; Njabon, R. N.; Tian, Z. R. *J. Am. Chem. Soc.* **2006**, *128*(33), 10960.
(11) Zhao, A.; Liang, J.; Xiong, Z.; Qian, Y. *Chem. Lett.* **2007**, *36*(3), 432–433.
(12) Yang, P.; Greene, L. E.; Law, M. U.S. Pat. Appl. Publ. US 2005009224, 2004-868421.

Published on Web 05/19/2009

which apical oxygens in one sheet form the array of basal oxygens for the corner-shared tetrahedral sheet above. The atomic arrangements on low index planes of the hexagonal prism on ZnO, **{10$\bar{1}$0}** and **{11$\bar{2}$0}** are stoichiometric, with equal numbers of exposed $^{IV}Zn^{2+}$ or $^{IV}O^{2-}$ ions, while the basal planes, (0001) and **(000$\bar{1}$)**, and the pyramidal planes, **{10$\bar{1}$1}**, are strongly polar, consisting of sheets of $^{IV}Zn^{2+}$ or $^{IV}O^{2-}$. The polar zinc-terminated surface is usually designated as (0001) and the polar oxygen-terminated surface as (000$\bar{1}$).[13]

ZnO has been produced with different morphologies by various synthetic methods. Vapor−liquid−solid (VLS) processes, chemical vapor deposition (CVD), and thermal evaporation are three methods that have been used for fabricating one-dimensional ZnO nanowires or wire arrays onto different substrates. There are many other approaches that have been used to achieve other ZnO nanostructures, such as hydrothermal methods,[14] solvothermal methods,[15] sol−gel processes,[16] laser-induced decomposition,[17] ultrasonic irradiation methods,[18] microwave irradiation techniques[19] and vapor phase transport.[20] Nanocombs, nanorings, nanohelices /nanosprings, nanobows, nanobelts, nanowires, and nanocages of ZnO have been synthesized using a solid-state thermal sublimation process by controlling the growth kinetics, local growth temperature, and the chemical composition of the source materials.[21] In addition, a nanosheet-based ZnO flower has been produced by simple precipitation followed by solvothermal treatment in the presence of ethanol.[22]

Hourglass-like ZnO nanostructures also have been prepared by a hydrothermal method with the assistance of polyoxyethylene[20] sorbitan trioleate, in which an ammonia solution was used as the precipitator and zinc nitrate as starting material.[23] A cornlike morphology of ZnO was synthesized under solvothemal-assisted heat treatment with zinc acetate as the zinc source.[24] Small ZnO tripodlike arms were assembled at the end of nanowires through the thermal evaporation of Zn powder in a horizontal tube furnace.[25] Hexagonal cone and column, nanobipyramid, and doughnut morphologies were fabricated by a solvothermal method when zinc nitrate was used as a starting material.[26−28] Tian et al.[10] developed a mild, aqueous solution-synthesis approach to hierarchical growth of complex and oriented ZnO nanostructures by taking advantage of the preferential adsorption of SDAs on different facets of hexagonal ZnO crystals. ZnO colloidal spheres with a narrow size distribution were produced in a sol−gel process.[16] Rodlike ZnO with various aspect ratios have also been made by a solvothermal treatment with zinc acetate in different organic solvents.[14,15] Laser-assisted decomposition is a newer technique for producing ZnO nanostructures.[17] Sonication and microwave irradiation were also helpful for preparing shape-selective ZnO nanostructures.[18,29,30]

Solution chemical routes, such as solvothermal, hydrothermal, and sol−gel processes, are very attractive because the synthesis conditions used are mild, and the processes are simple and inherently scalable; these factors make such processes much more economic than vapor phase methods. Zinc nitrate and zinc acetate have been widely used with wet chemical methods due to their higher solubility in water or other organic solvents. Zinc acetylacetonate is a common zinc source for the vapor transport method, such as CVD,[31] because of its ability to sublime. However, there are very few studies in which $Zn(AcAc)_2$ has been used as the zinc source in wet chemical processes.[32,33]

Because of the diverse range of morphologies that can be produced, and the various useful properties that ZnO can exhibit in these morphological states, ZnO materials have been used in transistors,[5] CO gas sensors,[34] nanogenerators,[7] UV sensors,[6] solar cells,[35] water splitting catalysts,[36] and photocatalysts[37] for decomposition of organic solution. The catalytic performance of nanocrystals is determined either by the composition in terms of the atomic structure[38] or by the morphologies that affect surface atomic arrangements and coordination.[39] For example, Pt with high-index planes showed extremely high catalytic reactivity because of the high density of atomic steps, ledges, and kinks, which in turn can serve as active sites for catalytic reactions.[40] For ZnO, the polar

(13) Woll, C. *Prog. Surf. Sci.* **2007**, *82*(2−3), 55.
(14) Cheng, B.; Samulski, E. T. *Chem. Comm.* **2004**, *8*, 986.
(15) Ayudhya, S. K. N.; Tonto, P.; Mekasuwandumrong, O.; Pavarajarn, V.; Praserthdam, P. *Cryst. Growth Des.* **2006**, *6*(11), 2446.
(16) Cheng, H.-M.; Hsu, H.-C.; Chen, S.-L.; Wu, W.-T.; Kao, C.-C.; Lin, L.-J.; Hsieh, W.-F. *J. Cryst. Growth* **2005**, *277*(1−4), 192.
(17) Fauteux, C.; Longtin, R.; Pegna, J.; Therriault, D. *Inorg. Chem.* **2007**, *46*(26), 11036.
(18) Jung, S.-H.; Oh, E.; Lee, K.-H.; Yang, Y.; Park, C. G.; Park, W.; Jeong, S.-H. *Cryst. Growth .Des.* **2008**, *8*(1), 265.
(19) Bhat, D. K. *Nanoscale Res. Lett.* **2008**, *3*(1), 31.
(20) Huang, M. H.; Wu, Y.; Feick, H.; Tran, N.; Weber, E.; Yang, P. *Adv. Mater.* **2001**, *13*(2), 113.
(21) Wang, Z. L. *Mater. Today* **2004**, *7*(6), 26.
(22) Pan, A.; Yu, R.; Xie, S.; Zhang, Z.; Jin, C.; Zou, B. *J. Cryst. Growth* **2005**, *282*(1−2), 165.
(23) Yao, K. X.; Sinclair, R.; Zeng, H. C. *J. Phys. Chem. C* **2007**, *111*(5), 2032.
(24) Yang, L.; Wang, G.; Tang, C.; Wang, H.; Zhang, L. *Chem. Phys. Lett.* **2005**, *409*(4−6), 337.
(25) Zhang, Z.; Liu, Y.; Liu, D.; Luo, S.; Shen, J.; Liu, L.; Ma, W.; Ren, Y.; Xiang, Y.; Zhou, W.; Xie, S.; Zheng, K.; Zhao, Y.; Sun, L.; Zou, C.; Yu, D. *Appl. Phys. Lett.* **2007**, *91*(1), 013106/1.
(26) Ghoshal, T.; Biswas, S.; Kar, S.; Chaudhuri, S.; Nambissan, P. M. G. *J. Chem. Phys.* **2008**, *128*(7), 074702/1.
(27) Ghoshal, T.; Kar, S.; Chaudhuri, S. *J. Cryst. Growth* **2006**, *293*(2), 438.
(28) Ghoshal, T.; Kar, S.; Chaudhuri, S. *Cryst. Growth Des.* **2007**, *7*(1), 136.
(29) Shao, H.; Qian, X.; Huang, B. *Mater. Lett.* **2007**, *61*(17), 3639.
(30) Cheng, J.; Zhang, Y.; Guo, R. *J. Cryst. Growth* **2008**, *310*(1), 57.
(31) Baxter, J. B.; Aydil, E. S. *J. Cryst. Growth* **2005**, *274*(3−4), 407.
(32) Yao, K. X.; Zeng, H. C. *J. Phys. Chem. B* **2006**, *110*(30), 14736.
(33) Inubushi, Y.; Takami, R.; Iwasaki, M.; Tada, H.; Ito, S. *J. Colloid Interface Sci.* **1998**, *200*(2), 220.
(34) Wang, J. X.; Sun, X. W.; Huang, H.; Lee, Y. C.; Tan, O. K.; Yu, M. B.; Lo, G. Q.; Kwong, D. L. *Appl. Phys. A: Mater. Sci. Process.* **2007**, *88*(4), 611.
(35) Jiang, C. Y.; Sun, X. W.; Lo, G. Q.; Kwong, D. L.; Wang, J. X. *Appl. Phys. Lett.* **2007**, *90*(26), 263501/1.
(36) Maeda, K.; Teramura, K.; Saito, N.; Inoue, Y.; Domen, K. *J. Catal.* **2006**, *243*(2), 303.
(37) Zheng, Y.; Chen, C.; Zhan, Y.; Lin, X.; Zheng, Q.; Wei, K.; Zhu, J.; Zhu, Y. *Inorg. Chem.* **2007**, *46*(16), 6675.
(38) Zhang, J.; Sasaki, K.; Sutter, E.; Adzic, R. R. *Science* **2007**, *315* (5809), 220.
(39) Narayanan, R.; El-Sayed, M. A. *Nano Lett.* **2004**, *4*(7), 1343.
(40) Tian, N.; Zhou, Z.-Y.; Sun, S.-G.; Ding, Y.; Wang, Z. L. *Science* **2007**, *316*(5825), 732.

planes are very important for catalyzing N-formylation reactions, because they favor formation of more oxygen vacancies.[41] In addition, some researchers have shown that the morphology of ZnO can play an important role in determining properties, which directly affect the catalytic performance.[9] However, the relationships between the morphology, crystal growth habit, and properties of ZnO nanomaterials have not been elucidated in detail. In particular, there have been no studies of the effect of ZnO nanocrystal morphology on catalytic properties.

In this paper, we report the synthesis of ZnO with different morphologies by simple solvothermal methods. Herein, zinc acetylacetonate was used as the zinc source in the solvothermal process for the first time. Solvents with different saturated vapor pressures aided in the production of ZnO nanomaterials with unique shapes. For comparison, a limited number of syntheses were performed using zinc acetate, instead of zinc actylacetonate, as the zinc source. The optical properties and the photocatalytic efficacy in phenol decomposition were also explored. ZnO materials with different crystal growth habits showed significant differences in catalytic performance for phenol photodegradation.

2. Experimental Section

2.1. Synthesis of ZnO. All reagents were analytical grade. In a typical synthesis, zinc acetylacetonate (3 mmol) was placed in a 22 mL Teflon linear with 14 mL solvent under vigorous stirring for 15 min (zinc acetylacetonate was more dispersed in organic solvents than in water), and the Teflon linear was then placed in a stainless steel autoclave. The sealed tank was put into an oven and heated at 120 °C for 20 h. When the reaction was complete, the autoclave was allowed to cool to room temperature. The white precipitate was separated by centrifuging, washed by centrifugation-redispersion with deionized distilled water and ethanol several times, and finally dried in air at 80 °C overnight. To investigate the effect of zinc source on the final product, we used zinc acetate as starting material and THF as the solvent. Other conditions are the same.

2.2. Characterization. *2.2.1 Structure*. The structure of the sample was determined by powder X-ray diffraction (XRD) using a Scintag XDS 2000 diffractometer with Cu Kα radiation ($\lambda = 0.1542$ nm) at a beam current of 40 mA.

2.2.2 Morphology. The crystal morphologies of the samples were investigated using a Zeiss DSM 982 Gemini field-emission scanning electron microscope (FESEM) with a Schottky emitter. Powder samples were dispersed in ethanol, dropped onto a gold-coated silicon wafer, and allowed to dry; the wafer was then mounted onto a stainless steel sample holder using silver conductive paint. Transmission electron microscopy (TEM) was also used to verify the morphology of the samples. TEM studies were carried out on a JEOL 2010 instrument with an accelerating voltage of 200 kV. The samples were prepared by dispersing the material in water. A drop of the dispersion was then placed on a carbon-coated copper grid and allowed to dry.

2.2.3. BET Surface Areas. N_2 physisorption was performed in a Micromeritics ASAP 2010 instrument to study surface area of the ZnO samples. Samples were pretreated by degassing at 120 °C overnight to remove any adsorbed species.

2.2.4. Optical Properties. The solid samples were dispersed in water and UV−vis spectra were measured from these dispersions using an HP 8452A Diode Array UV−vis spectrophotometer to detect absorption over the range of 200 to 820 nm. Room-temperature photoluminescence measurements were performed on the solid samples directly using a SLM AMINCO photoluminescence instrument with an excitation wavelength of 325 nm.

2.2.5. Photocatalytic Measurements. Each catalyst (50 mg) was suspended in 50 mL of phenol solution (12 ppm) in a quartz tube, and the mixture was then stirred for 20 min to attain equilibrium adsorption on the surface of the catalyst in the absence of UV light. During the photocatalytic reaction, vigorous stirring and a cooling fan were used to help the catalyst perform efficiently and to keep the system at room temperature, respectively. Six 15 W UV lamps ($\lambda = 254$ nm) were applied as the UV source. After a given reaction time, about 5 mL of mixture was withdrawn, and the solution was collected by filtration. The degradation process was monitored by a HP 8452A diode array UV−vis spectrophotometer (measuring the absorption of phenol at $\lambda = 210$ nm).

3. Results

3.1. XRD. X-ray diffraction (XRD) was used to investigate the phase purity of the synthesized ZnO, as shown in Figure 1. The standard diffraction data for ZnO are also shown for comparison (rod pattern at the bottom of Figure 1). All of the diffraction peaks from the samples corresponded to those of ZnO with the hexagonal wurtzite structure. The relative intensities of most of the peaks are in good agreement with those in the JCPDS file for wurtzite-structure ZnO (JCPDS: 36−1451), the main exceptions being peaks (**10$\bar{1}$0**) and (0002) in (e), whose relative intensity is quite different from that expected from the JCPDS data. There are XRD line broadenings for the samples prepared in THF, ethanol, and acetone solvents, which suggested a smaller crystallite size in these samples. No impurity peaks were observed for any of the synthesized samples.

3.2. FE-SEM. The ZnO materials synthesized in different solvents had rather different morphologies, as shown in Figure 2. In general, ZnO formed hexagonal shapes, such as cones and columns,[27] microprisms,[42] and microtubes,[43] which are consistent with the hexagonal crystal structure of ZnO.

(41) Li, G. R.; Hu, T.; Pan, G. L.; Yan, T. Y.; Gao, X. P.; Zhu, H. Y. *J. Phys. Chem. C* **2008**, *112*(31), 11859.

(42) Yu, S.-Y.; Zhang, H.-J.; Peng, Z.-P.; Sun, L.-N.; Shi, W.-D. *Inorg. Chem.* **2007**, *46*(19), 8019.

(43) Wei, A.; Sun, X. W.; Xu, C. X.; Dong, Z. L.; Yang, Y.; Tan, S. T.; Huang, W. *Nanotechnology* **2006**, *17*(6), 1740.

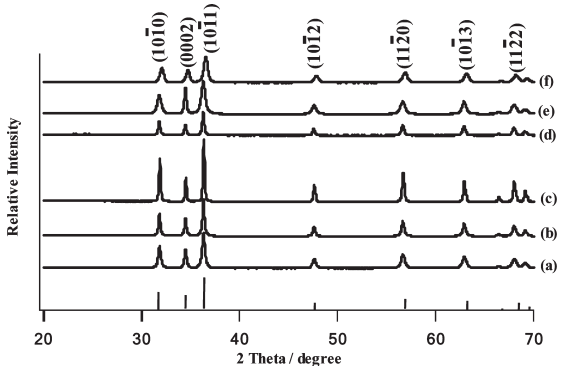

Figure 1. XRD patterns of the as-synthesized samples in different solvents: (a) THF, (b) decane, (c) H_2O, (d) toluene, (e) ethanol, and (f) acetone.

ZnO synthesized in THF solvent exhibited a cauliflower-like morphology, and most of the cauliflowers were attached to one another through the stem, as shown in Figure 2a. The size of the cauliflowers was on the scale of micrometers. Each cauliflower consisted of aggregates of nanoparticles with sizes of 15−25 nm, and most of the nanoparticles did not have obvious facets, as shown in images a and b in Figure 2.

When decane was used as the solvent, the synthesized ZnO had a truncated hexagonal conical morphology, as shown in images c and d in Figure 2. According to Figure 2d, the truncated planes on each crystal were smooth. The height of the cones was around 1 μm, the side length of the top hexagonal face was between 300 and 400 nm, and the side length of the bottom hexagonal face was between 700 nm and 1 μm. A few cones were joined across the basal plane to make hourglass-shaped particles, as shown in the lower insert to Figure 2c.

Images e and f in Figure 2show that rodlike ZnO was synthesized when only water was used as the solvent; upon closer examination of the morphology, it is clear that some of the rods were hollow. The diameters of the rods and tubes varied a great deal, from 200 to 500 nm. Both rods and tubes exhibited hexagonal cross-sections.

Images g and h in Figure 2show that in toluene solvent, ZnO with hourglasslike shapes was obtained. The height of these hourglasslike particles was around 1.2 μm. The bottom of the hourglass was hexagonal with a side length of 500 nm, as revealed in Figure 2h. The surfaces of the hourglasslike particles were rough. More details of this morphology are discussed below in the section on HR-TEM.

Rodlike ZnO was also synthesized with ethanol as the solvent. The length of the rods was around 250 nm, and the diameter was around 30 nm. As shown in images I and j in figures 2, the rods tended to connect with each other through the center to form a radial shape.

Spherical ZnO was obtained when acetone was used as the solvent, as shown in images k and l in Figure 2. The sizes of the spheres varied from 750 nm to 1 μm. Upon closer observation, the spherical structures seemed to comprise nanoparticles 30−50 nm in diameter as shown in Figure 2l.

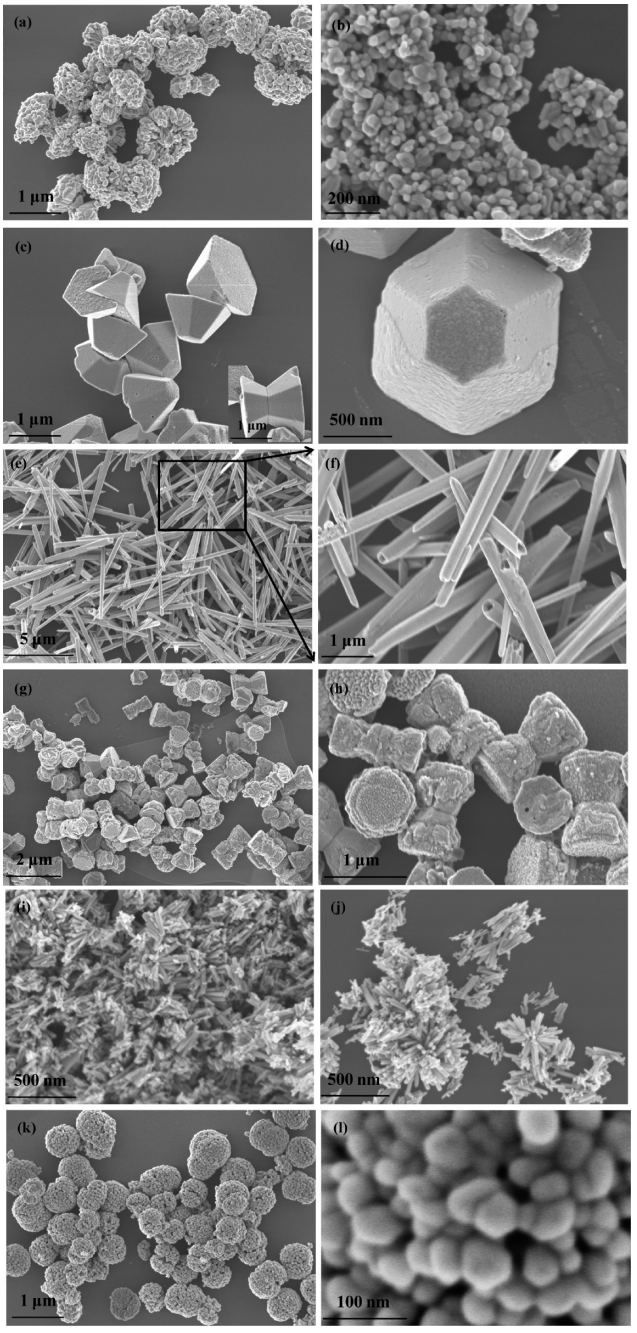

Figure 2. FE-SEM images of the as-synthesized samples in different solvents: (a, b) THF; (c, d) decane; (e, f) H_2O; (g, h) toluene; (i, j) ethanol; (k, l) acetone.

3.3. TEM. Figure 3a−c shows bright-field images of ZnO prepared in THF solvent. Figure 3d is an HR-TEM phase contrast image with a beam direction of [**11$\bar{2}$0**]. TEM observations in Figure 3 showed that the cauliflower-like ZnO are comprised of nanoparticles with no well-defined crystallographic facets. These nanoparticles contained high densities of stacking faults on (0001).

Figure 4 is a group of TEM images and selected area diffraction (SAED) patterns of the ZnO prepared in decane solvent. The ZnO crystals exhibit truncated hexagonal conical shapes, having **{1$\bar{1}$01}** planes as the side planes and {0001} planes as the top and bottom planes, as shown in images a and b in Figure 4. Some of the

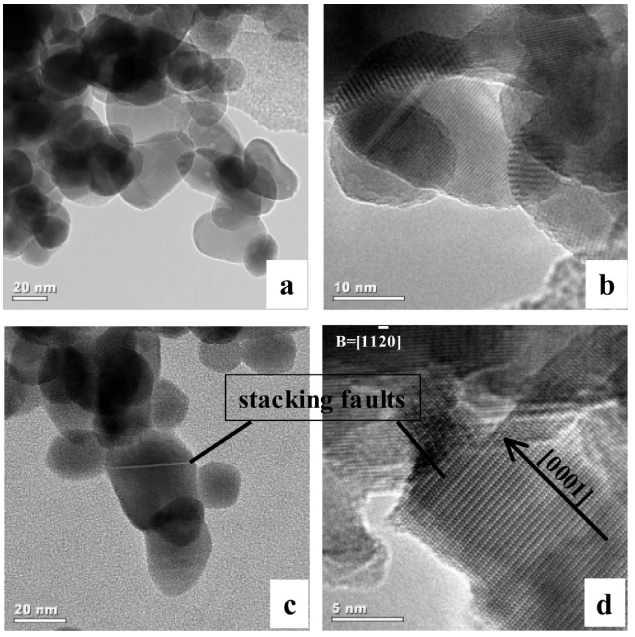

Figure 3. HR-TEM images and SAED of ZnO prepared in THF solvent.

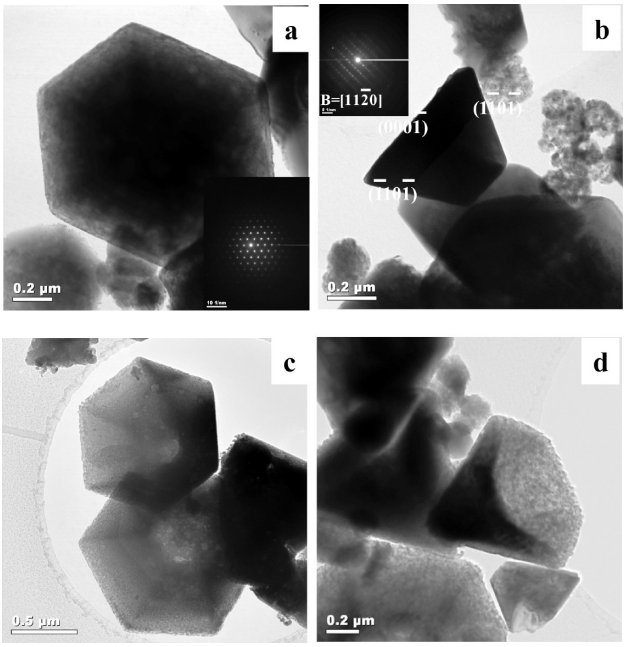

Figure 4. HR-TEM images and SAED of ZnO prepared in decane solvent.

truncated hexagonal cones have interior cavities, as revealed in images c and d in Figure 4.

The TEM data in Figure 5 confirm the coexistence of rods and tubes for the ZnO particles prepared in water. Both the rods and tubes have their major axes parallel to [0001], as shown in the SAED patterns (patterns b and d in Figure 5).

Figure 6 contains TEM images and SAED patterns of hourglass-like ZnO prepared with toluene solvent. The HR-TEM images and SAED patterns reveal that the hourglasslike ZnO particles grow along [0001]. Electron diffraction pattern in Figure 6b corresponds to the area labeled as 1′ in Figure 6a, and the electron diffraction pattern in Figure 6d corresponds to the area labeled as 2′

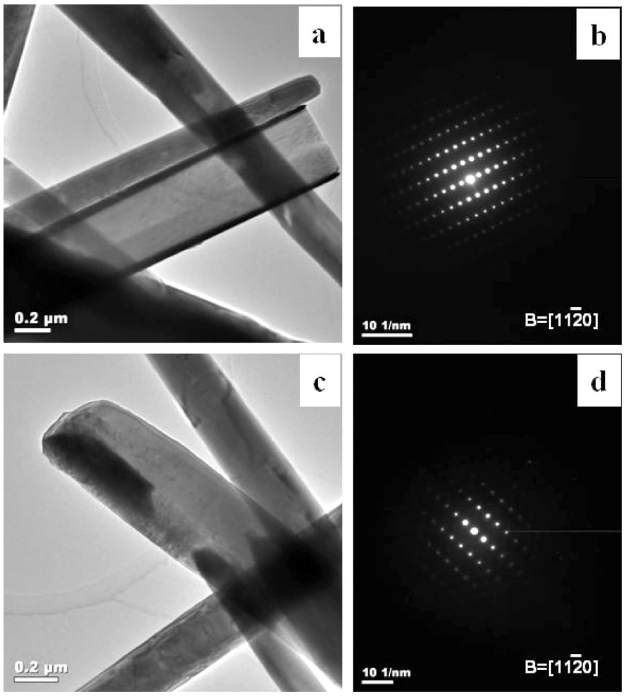

Figure 5. HR-TEM images and SAED of ZnO prepared in water solution.

in Figure 6c. However, there is a splitting of the (000*n*) reflections in the patterns obtained from regions in the "necks" of the hourglass structures (e.g., in the areas labeled as 1′ in Figure 6a and 2′ in Figure 6c), indicating that there is a slight misorientation between the crystals in the two parts of each hourglass. Figure 6e is a HR-TEM image of the surface of one hourglass crystal. Such images show that there is pronounced roughness on the surface at an atomic scale but that these features have the same lattice orientation as the body of the crystals.

Figure 7 is a series of TEM images from rodlike ZnO prepared with ethanol solvent. Figure 7a shows the aggregation of the rods through the ends to form the radial morphology. Stacking faults are clearly observed on (0001), as shown in Figure 7b−e.

Spherical ZnO was obtained in acetone solvent. These spheres comprised nanoparticles with diameters of 20−50 nm, as shown in images a and b in Figure 8. The nanoparticles exhibited obvious crystallographic facets, as shown in images b and c in Figure 8. On the basis of the [**1$\bar{2}$13**] zone-axis SAED pattern in the inset to Figure 8d, the planes of the nanoparticle facets were indexed as (**10$\bar{1}$0**) and (**$\bar{1}$101**). There were no stacking faults observed in the high-resolution TEM images from these nanoparticles (e.g., Figure 8d).

3.4. Optical Properties. UV−vis absorption and room-temperature photoluminescence were used to study the optical properties of the as-synthesized ZnO. The UV−vis absorption spectra of all of the ZnO samples dispersed in distilled deionized water are shown in Figure 9. The sample obtained when ethanol was used as the solvent showed a well-defined exciton band at 370 nm, which is corresponding to the bulk ZnO

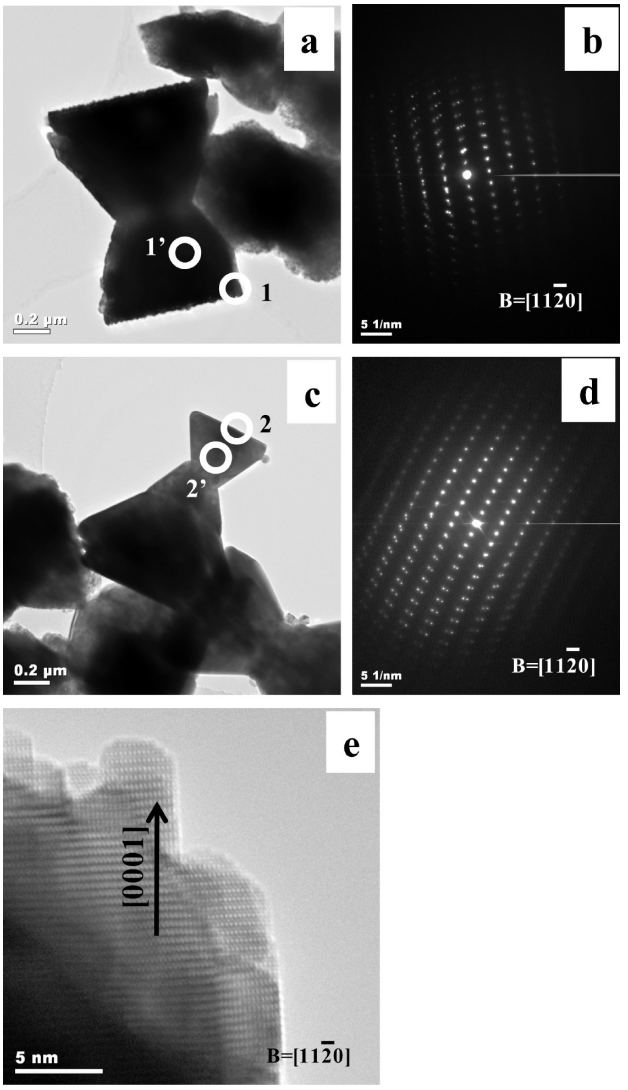

Figure 6. HR-TEM images and SAED of ZnO prepared with toluene as solvent.

absorption.[22] ZnO samples synthesized in THF and decane showed similar UV−vis absorption curves, with absorptions around 380 nm that were red-shifted relative to the bulk exciton absorption at 370 nm. The factors that caused red-shifts of UV−vis absorption bands are under investigation.

Besides the ultraviolet absorption, these two samples also showed red absorption from 650 to 800 nm, as shown in spectra a and b in Figures 9. UV absorption of ZnO samples prepared when acetone and water were used as solvents behaved very similarly. ZnO synthesized in toluene solvent showed unique UV absorption, compared with other materials. There was obvious broad visible absorption, as shown in Figure 9d, besides the UV absorption located at around 386 nm. The absorption in the visible spectral range suggested that more absorption states or defect energy bands exist in the as-synthesized ZnO samples.[27] In spite of showing excitonic characteristics in all the absorption spectra, an asymmetric tail was observed toward the higher wavelengths because of scattering. ZnO samples were insoluble in water. An appreciable amount of light was always

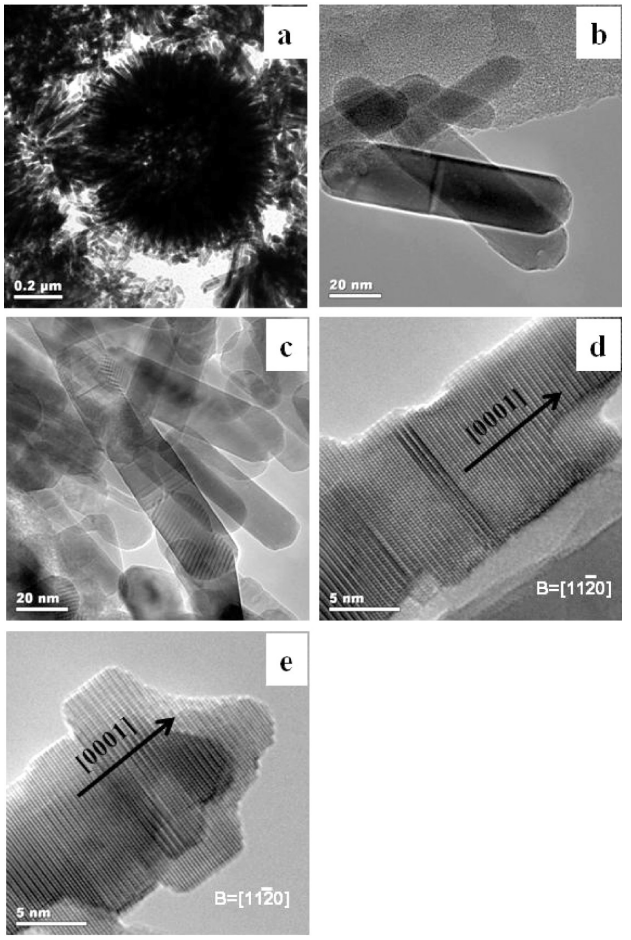

Figure 7. HR-TEM images and SAED of ZnO prepared with ethanol as solvent.

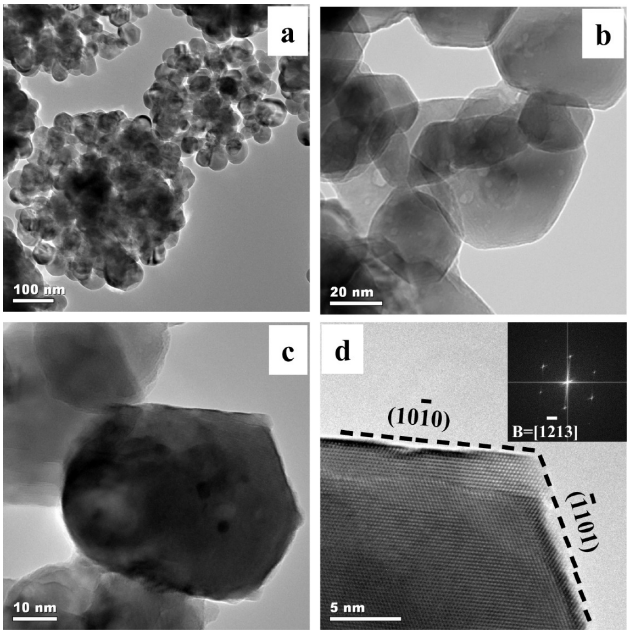

Figure 8. HR-TEM images and SAED of ZnO prepared with acetone as solvent.

scattered by the dispersions because of the inhomogeneous distributions of the particles.[27]

Room-temperature photoluminesence spectra with an excitation wavelength of 325 nm were measured to further

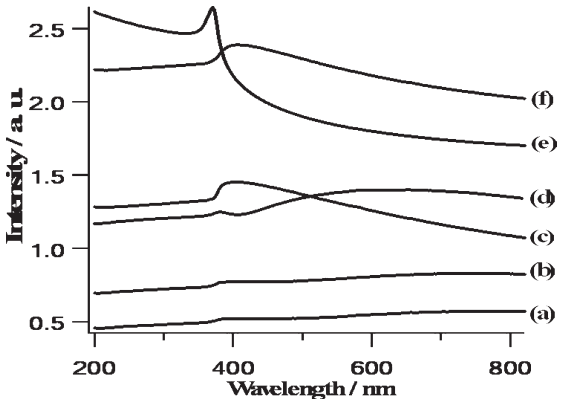

Figure 9. UV−vis absorption spectra of the as-synthesized samples in different solvents: (a) THF, (b) decane, (c) H_2O, (d) toluene, (e) ethanol, and (f) acetone.

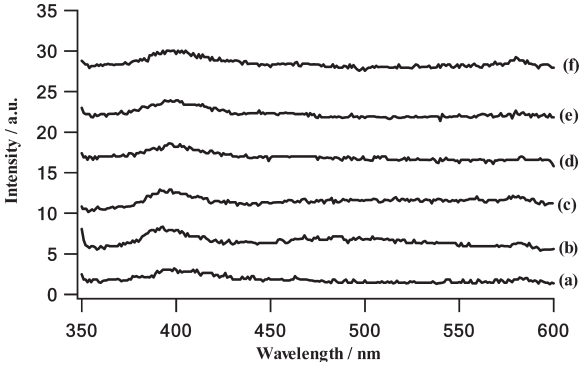

Figure 10. Room-temperature photoluminescent spectra of the as-synthesized samples in different solvents: (a) THF, (b) decane, (c) H_2O, (d) toluene, (e) ethanol, and (f) acetone.

characterize the defect features of these ZnO samples. All of the ZnO samples synthesized with different solvents displayed UV emission peaks with maxima at around 390 nm, which is ascribed to the excitonic recombination corresponding to the band edge emission of ZnO samples,[42,44] as shown in Figure 10. The presence of the UV emission at room temperature confirms the excellent crystallinity of the ZnO materials. ZnO samples produced in THF, decane, water, and acetone also showed a weak emission at around 575 nm, which was designated green emission. This green emission originates from the radiative recombination of photogenerated holes with electrons occupying oxygen vacancies.[20]

3.5. Phenol Photodegradation. ZnO has been used as a photocatalyst for the photodegradation of water pollutants, photoreduction of halogenated benzene derivatives, photoreduction of toxic metal ions, and photocatalytic water splitting. To understand the relationship between the structure and photocatalytic performance of ZnO samples, the photocatalytic activities of as-synthesized ZnO with different morphologies were studied using the degradation of solutions of phenol. Figure 11 shows a schematic illustration of the photodegradation setup. Photodegradation of phenol is a first order reaction. Figure 12 shows the photodegradation

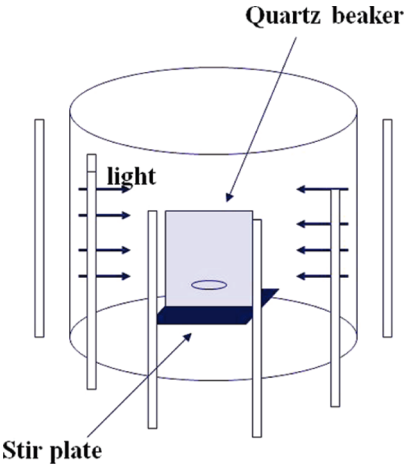

Figure 11. Schematic of phenol photodegradation setup.

results for phenol on the ZnO catalysts. Figure 12I shows the kinetic plots with first order linear plots of $\ln C_0/C = f(t)$, in which C_0 and C are the initial concentration after the equilibrium adsorption and the reaction concentration of phenol, respectively. Time-dependent photoactive performance of ZnO catalysts for phenol degradation was recorded, as shown in Figure 12II. Degradation (Y axis), is defined as $(1 - C/C_0) \times 100\%$, and the X axis is reaction time (min).

The degradation rates of phenol showed large differences for ZnO synthesized with different morphologies. The activity of the ZnO catalysts was evaluated by comparing the first order rate constant (k). ZnO obtained in THF solvent showed the best catalytic performance, and the kinetic rate constant k is 0.1496 min^{-1}, as shown in Figure 12I-a. Phenol was almost totally degraded after exposure under ultraviolet light for 20 min, as shown in Figure 12II-a. ZnO synthesized with decane solvent was also an excellent catalyst for phenol degradation (k = 0.0867 min^{-1}). Phenol was totally degraded in half an hour with this catalyst. ZnO obtained in water and toluene solvents (curves c and d) showed higher activity for phenol degradation (k = 0.0651 and 0.0518 min^{-1}, respectively) at the beginning of the exposure under UV light than for ZnO in ethanol solvent (k = 0.0468 min^{-1}). However, total degradation of phenol took a shorter time on ZnO produced in ethanol than on samples c and d. ZnO prepared with acetone as solvent showed the lowest activity of all of the synthesized ZnO materials, with k = 0.0385 min^{-1}, but even this is more than twice the rate constant of commercial ZnO (0.0182 min^{-1}). The commercial ZnO with surface area 1.5 m^2/g was bought from Fisher. The morphology of the commercial ZnO was shown in Figure 13. For comparison, the phenol solution was exposed under UV light without any catalyst, as shown in Figure 12II h, and no degradation was observed. The best catalyst, ZnO prepared in THF solvent, showed 9 times enhancement in activity as compared to commercial ZnO.

3.6. XRD and FE-SEM of ZnO with Zinc Acetate as Precursor. The XRD pattern of ZnO prepared with zinc acetate as the zinc precursor showed that pure ZnO with

(44) Huang, M. H.; Wu, Y.; Feick, H.; Tran, N.; Weber, E.; Yang, P. *Adv. Mater.* **2001**, *13*(2), 113.

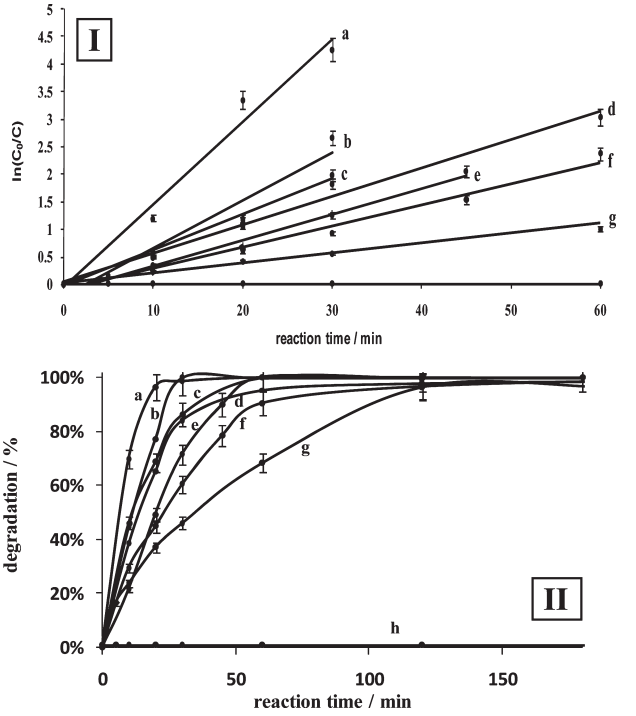

Figure 12. (I) Kinetic plots with first-order linearity of $\ln C_0/C = f(t)$ and (II) performance of the catalysts for phenol photodegradation: (a) THF, (b) decane, (c) H_2O, (d) toluene, (e) ethanol, (f) acetone, (g) commercial ZnO, and (h) without catalyst.

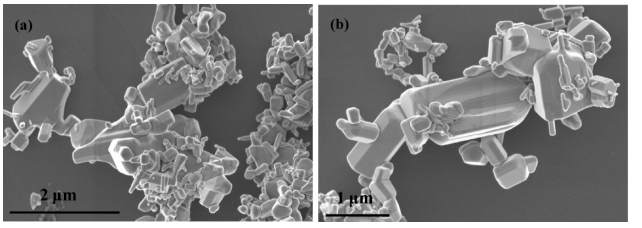

Figure 13. FE-SEM images of the commercial ZnO.

the hexagonal wurtzite structure was obtained; no impurities were observed. Therefore, the choice of zinc precursor did not affect the crystal structure, as shown in Figure 14 and Figure 1. FE-SEM data were used to investigate the morphologies of ZnO samples prepared with different precursors. Hexagonal pyramidal ZnO was obtained, as shown in Figure 15. The sizes of the pyramids were not homogeneous, and varied from 200 nm to 1 μm.

4. Discussion

4.1. Effects of Solvents on the Morphologies of ZnO Materials. Crystallization and growth of ZnO under solvothermal conditions were mainly determined by the intrinsic crystal structure and external reaction conditions. In ZnO with the wurtzite structure, divalent Zn^{2+} ions occupy the tetrahedra formed by O^{2-} ions, and the tetrahedra connect with each other via corner-sharing. Consequently, wurtzite ZnO can be described as layers of Zn^{2+} and O^{2-} ions stacked alternately along the [0001] direction (*c*-axis), which results in a polar ZnO crystal structure. There is a variety of external factors that can have a strong impact on the solvothermal growth of crystals; these can be grouped into chemical factors and

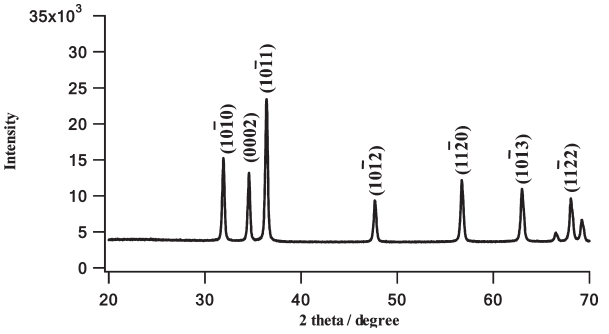

Figure 14. XRD pattern of the sample with zinc acetate as the zinc precursor.

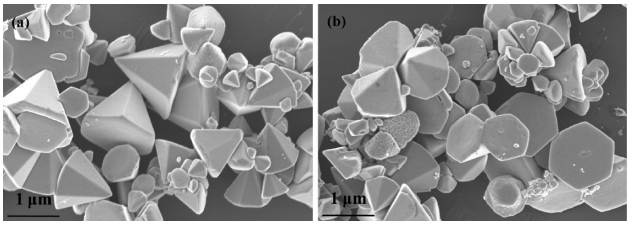

Figure 15. FE-SEM images of the sample with zinc acetate as the zinc precursor.

thermodynamic factors.[45] The main chemical factors are the choice of precursors and solvents for a particular process. The thermodynamic factors include the experimental conditions, such as temperature and pressure, which can affect the reaction mechanisms. In this study, zinc acetylacetonate was used as the zinc source, and reaction conditions (temperature and time) were kept the same for all of the reactions; the only significant difference between the samples is the solvent used. Therefore, the differences in the morphologies of the various synthesized ZnO materials can only be due to the effects of the different solvents.

4.1.1. Solubility of the Precursors in the Solvents. It has been shown previously that the choice of solvent can have a profound influence on the solvothermal growth of polar crystals.[14] Solvents with different polarities and saturated vapor pressures affect the morphology of samples synthesized under solvothermal treatment by adjusting the solubility of the precursor in the particular solvent, initial nucleation, agglomeration, and preferred orientation of the crystals.[46] In this study, zinc acetylacetonate ($Zn(AcAc)_2$) was used as the zinc source in solvothermal growth of ZnO for the first time. In these experiments, six solvents were used. Because of the large organic ligand (actylacetonate group) of the zinc source, the dispersion of the precursor in organic solvents was much better than in water. This effect resulted in the morphology of the ZnO materials synthesized in water being less homogeneous than that for ZnO materials prepared in organic solvents. For instance, ZnO synthesized in an ethanol solvent exhibited a nanorod morphology with a uniform aspect ratio. However, ZnO synthesized in water exhibited a microrod morphology with a large range of aspect ratios.

(45) Demazeau, G.; Goglio, G.; Largeteau, A., Mater. Res. Soc. Symp. Proc. 2005, 878E, Y1 4 1.
(46) Zhang, J.; Sun, L.; Yin, J.; Su, H.; Liao, C.; Yan, C. *Chem. Mater.* **2002**, *14*(10), 4172.

4.1.2. Polarity of the Solvents. The polarity of solvents influences not only the nucleation of the ZnO crystals but also the preferential direction of crystal growth.[14,15,46] Ayudhya[15] reported that solvents with lower polarity helped to cultivate rods with high aspect ratios, when zinc acetate was used as the Zn source. As shown in Figures 2a and 14a, the morphologies were strongly dependent on the precursors used; this is consistent with the conclusions drawn previously by Zhang et al.[46] Our findings on the effects of solvent polarity are, however, different from other reports;[14,15] this is presumably due to differences between the zinc actylacetonate precursor used here and the zinc acetate used in the previous studies. The solvents used in this study had widely varying polarities. This can be seen most easily from the dielectric constants of the solvents, with a higher dielectric constant corresponding to a higher polarity. The dielectric constants of water, ethanol, acetone, THF, toluene, and decane are 80.1, 25.3, 21.01, 5.6, 2.38, and 2.0,[47] respectively. In general, crystal growth habit depends on interface−solvent interactions.[15] ZnO is a polar crystal and the relative growth rates of the various crystal planes are different in solvents with different polarities. In solvents with high polarities, such as water and ethanol, the growth along the [0001] direction was enhanced, which resulted in rodlike morphologies. This implies that there is a strong interaction between the polar (0001) surface and the polar solvents, promoting the rate of crystal growth perpendicular to this surface. In lower polarity solvents, the interactions would be weaker, leading to less anisotropic growth rates and more equi-axed ZnO crystals.

4.1.3. Saturated Vapor Pressure of the Solvents. There are two main factors that contribute to the morphology of the final products obtained under solvothermal conditions: these are the initial nucleation of the crystals, and the solubility of the precursor in the solvents with different saturated vapor pressures.[48] The saturated vapor pressure is inversely related to the boiling point of the solvents. The boiling points of decane, toluene, water, THF, ethanol, and acetone are 174.15, 110.63, 100, 88, 78.29, and 56.05 °C, respectively. The saturated vapor pressure of the solvents follows the reverse order.

In this study, when THF, ethanol, and acetone were used as the solvents, aggregates of nanoparticles were formed. The saturated vapor pressure of acetone and THF is high, and growth of the ZnO nuclei was limited under the high-pressure conditions. This led to more extensive nanoparticle nucleation. The aggregation of these nanoparticles and the formation of clusters took place to reduce the overall surface area and thus to lower the surface energy of the sample. When solvents such as decane, toluene, and water were used, which have relatively low saturated vapor pressures, larger ZnO crystals with faceted morphologies were obtained. This implies that the lower saturated vapor pressures allow for more rapid growth of the ZnO nuclei, resulting in larger particles. Therefore, the saturated vapor pressure of the solvent used played a crucial role in the formation of different crystal morphologies.

4.1.4 Possible Growth Mechanism in Different Solvents. Nanoparticles grew both in THF and acetone solvent, but the particles showed different crystal growth habits. The extent of the aggregation for ZnO nanoparticles synthesized in acetone was greater than in THF, because sonication could break the cauliflower morphology, as shown in images a and b in Figure 3. The spherical morphologies were still retained after sonication, as shown in Figure 8a. One possible reason why the crystals grew differently in THF and acetone is because of the polarity of the solvents. Solvents with different polarities have different chelating effects with the metal cations, which may cause different crystal growth habits.

Because of the structural anisotropy and surface electric polarity of ZnO, the growth rates (r) along different crystal directions are r[0001] > r**[10$\bar{1}\bar{1}$]** > r**[10$\bar{1}$0]** > r**[10$\bar{1}$1]** > r**[000$\bar{1}$]** under normal conditions.[32] The mechanism of formation for faceted morphologies involves the disappearance of faster growing faces leaving crystals bound by slower growing faces. This effect was observed most clearly here for the truncated hexagonal ZnO cones that were fabricated in decane solvent. As claimed in the literature, [32] the planes **{01$\bar{1}$1}** have lower surface energies and are more stable than the higher energy polar planes. To minimize the total surface energy, the dissolution of the polar planes, such as (0001), is faster than that of the nonpolar planes. This may be why interior cavities were formed in ZnO with decane as the solvent.

Hourglasslike ZnO was produced with toluene as the solvent. Two different mechanisms have been proposed for the formation of this remarkable morphology in ZnO:[32] (i) direct coupling of two separate crystals across the (0001) planes, (ii) in situ nucleation and growth processes. No evidence for the in situ growth of the other halves was observed in our HR-TEM experiments (e.g., Figure 6); therefore, the hourglasslike morphology probably formed by direct coupling of two isolated crystals across the (0001) planes at the top of truncated pyramids. This is consistent with the SAED data that showed splitting in the 000*n* reflections; no such effects would be expected for the in situ growth mechanism.

For the solvothermal synthesis of ZnO in ethanol, the initial nucleation of ZnO crystals should be similar to that for ZnO produced by hydrothermal processes. [15] Ethanol also has a hydroxyl group, which had an important influence on ZnO nucleation under hydrothermal treatment. However, the further growth of ZnO crystals in ethanol was different from that in water, possibly because of the different saturated vapor pressures. In addition, nonpolar planes with lower surface energies were more stable than the higher-surface-energy polar planes.[49−51]

(47) Lide, D. R. Handbook of Chemistry and Physics; CRC Press: New York, 2004−2005; p 15.
(48) Biswas, S.; Kar, S.; Chaudhuri, S. *Mater. Sci. Eng., B* **2007**, *142* (2−3), 69.
(49) Li, F.; Ding, Y.; Gao, P.; Xin, X.; Wang, Z. L. *Angew. Chem., Int. Ed.* **2004**, *43*(39), 5238.
(50) Cho, S.; Jung, S.-H.; Lee, K.-H. *J. Phys. Chem. C* **2008**, *112*(33), 12769.
(51) Vayssieres, L.; Keis, K.; Hagfeldt, A.; Lindquist, S.-E. *Chem. Mater.* **2001**, *13*(12), 4395.

To minimize the total surface energy, the dissolution of the (0001) planes was faster than that for the nonpolar planes.[49] This is a possible reason for formation of tubular ZnO with water as the solvent.

4.2. Influence of the Morphologies on the Catalytic Performance of the ZnO Materials. The morphologies of ZnO catalysts play an important role in the photocatalytic activity;[41,52] this arises from differences in surface areas, polar planes, or oxygen vacancies as discussed below.

4.2.1. Influence of Surface Area on the Photocatalytic Activity. Usually, a high specific surface area has a beneficial effect on the activity for catalysts. High-surface-area ZnO hollow spheres[53] showed considerably higher photocatalytic activity for the degradation of dyes than commercial ZnO. However, in other studies,[41,54] higher surface areas of the catalysts did not result in higher catalytic performance. In this work, the surface areas of the ZnO materials prepared in THF, decane, water, toluene, ethanol, and acetone are 3.3, 2.5, 3, 3, 28.7, and 11.8 m^2/g, respectively. However, the catalytic performance followed the order of THF, decane, water, toluene, ethanol and acetone. Thus, there was no correlation between the surface areas and the catalytic activity data for our materials demonstrating that there are other more important factors that govern activity, such as crystal habits.[54]

4.2.2. Effects of the Crystal Habits on the Photocatalytic Performance. Catalysts with higher surface energy show better catalytic performance.[38,41] The growth of crystals with some preferred structures or planes was controlled by the surface energy of the planes, and the planes with lower surface energy were liable to dominate over the others. Two ways to reduce the surface energy are the agglomeration of particles to form clusters, or the formation of facets with different surface energy. Nonfaceted particles have higher surface energies than the faceted ones.[48] The surface energies (E) of the facets in ZnO crystals follow the sequence $E(0001) > E(10\bar{1}\bar{1}) > E(10\bar{1}\bar{0}) > E(10\bar{1}1) > E(000\bar{1})$, which is the same order as the crystal growth rates. ZnO prepared in THF showed the best catalytic activity among all of the ZnO samples synthesized, presumably because of the formation of nonfaceted nanoparticles in this sample. The conical ZnO prepared in decane solvent showed better activity than hourglasslike ZnO synthesized in toluene, although these morphologies exhibited similar crystal facets. There are two possible reasons for this effect: first, the conical ZnO exhibited larger areas of (0001) planes, because the two halves of the hourglass-shaped crystals attached through (0001) planes; second, the interior cavities in the conical ZnO can also play very important roles during photocatalysis.[54] Multiple reflection of UV light within the interior cavities may occur,[54] which allows for more efficient use of the incident light, and therefore offers an improved catalytic activity. Micrometer-sized rodlike ZnO synthesized in water showed better activity than nanorodlike samples synthesized in ethanol, presumably because of the tubular morphology. ZnO prepared when acetone was used as the solvent showed the least catalytic activity. This is due to the formation of nanoparticles with smooth ($\bar{1}101$) and ($10\bar{1}0$) facets, which did not have higher energy, resulting in poor activity.

4.2.3. Effects of Oxygen Vacancies on the Photocatalytic Activity. As reported in the literature, differences in photocatalytic activity are related not only to the surface adsorption ability but also to the type and concentration of oxygen vacancies on the surface.[37,55,56] Among the ZnO materials synthesized in this study, the samples prepared in THF, decane, water, and acetone had oxygen vacancies, as indicated by the photoluminescence data. Moreover, the existence of high densities of (0001) stacking faults in ZnO synthesized in ethanol may indicate that there were also oxygen vacancies in these materials.[57] Upon closer examination of the HR-TEM images in Figures 3d and 7d, it appears that there are differences in the stacking faults for ZnO produced in THF and in ethanol. Although further work is required to verify this, it is tempting to speculate that these differences may reflect differences in the oxygen vacancies for these materials. We note, however, that no stacking faults were observed in the ZnO material prepared in acetone, even though the photoluminescence data showed that there were oxygen vacancies present. Therefore, the concentrations of oxygen vacancies may be different in the ZnO materials synthesized using different solvents. Temperature-programmed desorption of O_2 experiments are underway to identify the types and the concentrations of the oxygen vacancies in the different ZnO materials.

5. Conclusion

In this work, it was demonstrated that the solvothermal process is an efficient approach for the preparation of wurtzite-structure ZnO with different morphologies in different solvents. Zinc acetylacetonate was used for the first time to fabricate ZnO with solvothermal methods. FE-SEM images showed that cauliflower-like, truncated hexagonal conical, nanospherical, nanorods, tubular, and hourglasslike ZnO were synthesized in THF, decane, acetone, ethanol, water, and toluene, respectively. The saturated vapor pressure of the solvents played an important role in controlling the morphology. The solvents with higher saturated vapor pressures tended to result in ZnO with an agglomerated nanoparticulate morphology. However, the samples synthesized in solvents with lower saturated vapor pressures tended to form relatively large crystals with faceted morphologies. All of the samples showed UV absorption and displayed UV emission at

(52) Lu, F.; Cai, W.; Zhang, Y. *Adv. Funct. Mater*. **2008**, *18*(7), 1047.
(53) Deng, Z.; Chen, M.; Gu, G.; Wu, L. *J. Phys. Chem. B* **2008**, *112*(1), 16.
(54) Li, H.; Bian, Z.; Zhu, J.; Zhang, D.; Li, G.; Huo, Y.; Li, H.; Lu, Y. *J. Am. Chem. Soc*. **2007**, *129*(27), 8406.
(55) Wang, Y.; Li, X.; Wang, N.; Quan, X.; Chen, Y. *Sep. Purif. Technol*. **2008**, *62*(3), 727.
(56) Sun, X.; Qiu, X.; Li, L.; Li, G. *Inorg. Chem*. **2008**, *47*(10), 4146.
(57) Gerthsen, D.; Litvinov, D.; Gruber, T.; Kirchner, C.; Waag, A. *Appl. Phys. Lett*. **2002**, *81*(21), 3972.

around 390 nm. All of the ZnO samples showed enhanced activity for photocatalytic phenol degradation; the material synthesized in THF exhibited a rate of 0.1496 min^{-1}, nine times that of commercial ZnO.

Acknowledgment. We thank the U.S. DOE, Office of Basic Energy Sciences, Division of Chemical Sciences, Geosciences, and Biological Sciences, for the support of this work. We thank Dr. Jim Romanow for the help with FESEM experiments in the Physiology and Neurobiology Department. We acknowledge Dr. Francis S. Galasso for helpful discussions. We thank Michale Duff for help with room-temperature photoluminescence experiments.